ISCI, Volume *16*

Supplemental Information

High-Throughput Screening of Solid-State Li-Ion Conductors Using Lattice-Dynamics Descriptors

Sokseiha Muy, Johannes Voss, Roman Schlem, Raimund Koerver, Stefan J. Sedlmaier, Filippo Maglia, Peter Lamp, Wolfgang G. Zeier, and Yang Shao-Horn

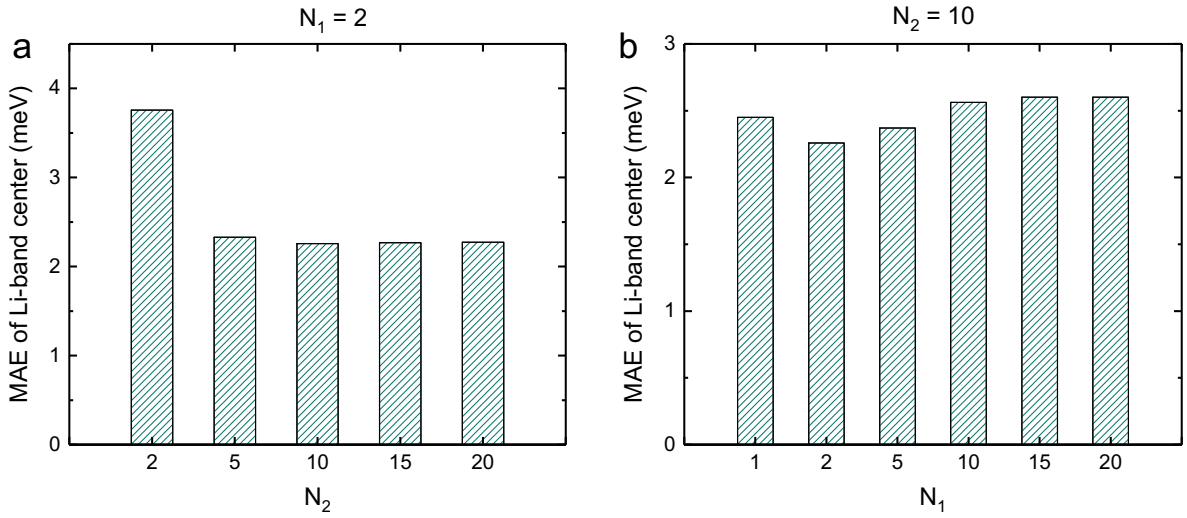

Figure S1. The mean absolute error of lithium-phonon band centers of the 53 compounds in Figure 2 as a function of the scaling parameter N_1 and N_2. Related to Figure 2.

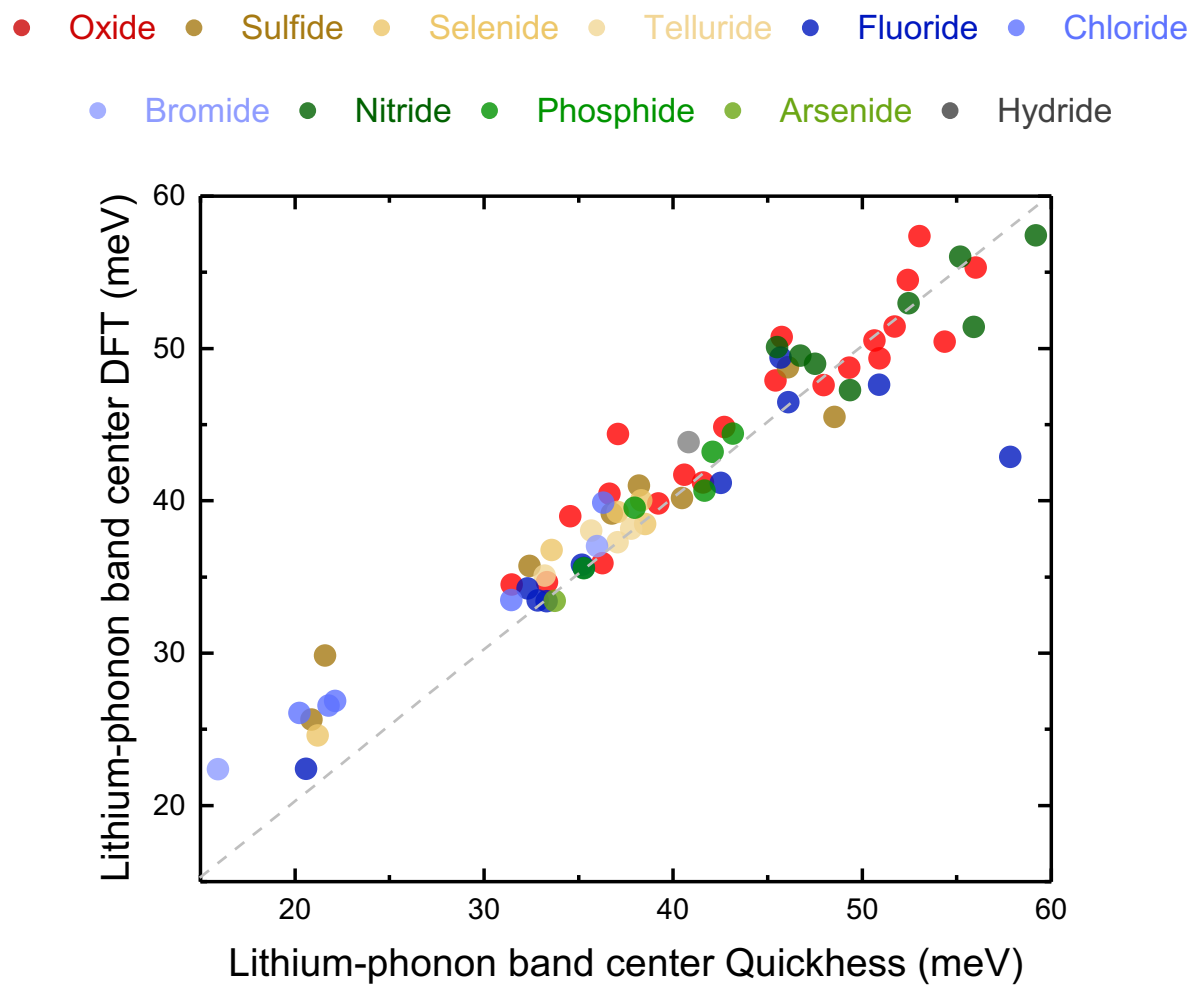

Figure S2. Comparison between the Li-phonon band centers of 71 compounds computed with *Quickhess* and full DFT calculations available in the Materials Project database. Related to Figure 2

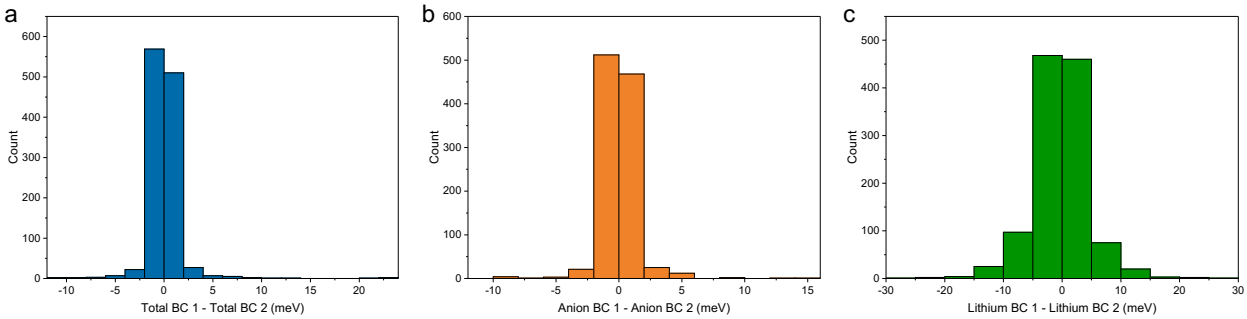

Figure S3. The difference between phonon band centers computed with two different sets of scaling parameters ($N_1 = 2$; $N_2 = 10$ and $N_1 = 5$; $N_2 = 10$) for all of the ~1200 compounds retained after pre-screening. Related to Figure 2 and 3.

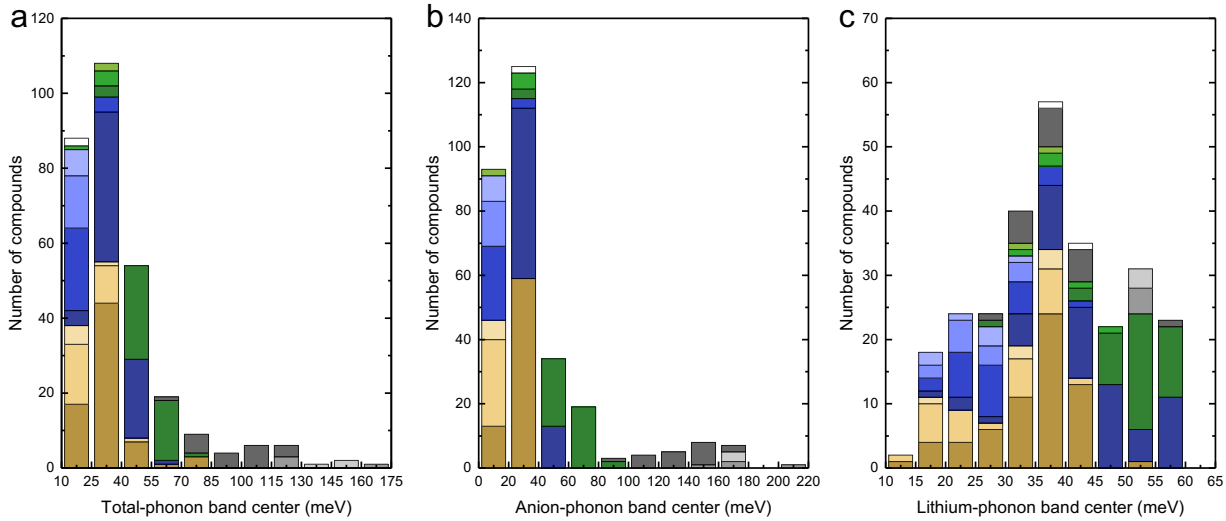

Figure S4. Histograms of a) Total-, b) Anion- and c) Lithium-phonon band centers for all chemistries excluding oxides. Related to Figure 3.

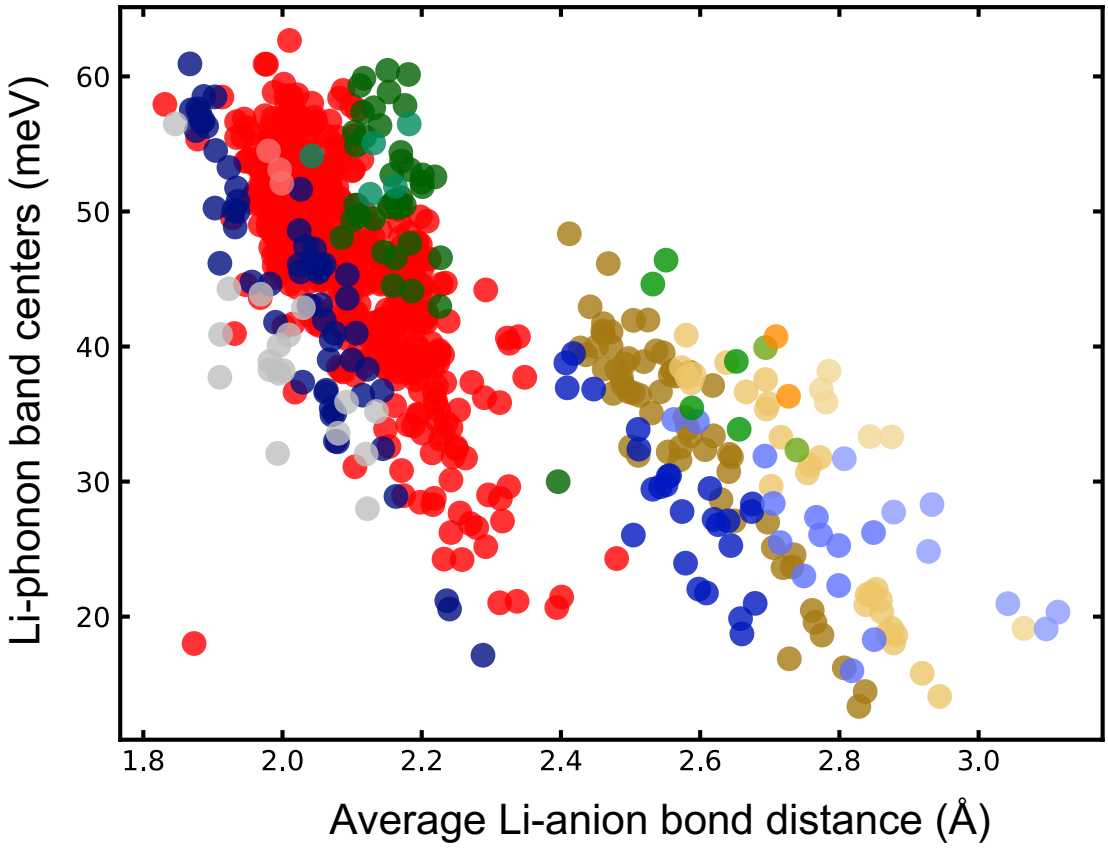

Figure S5. Correlation between the Li-phonon band centers and the average Li-anion bond length. Related to Figure 4.

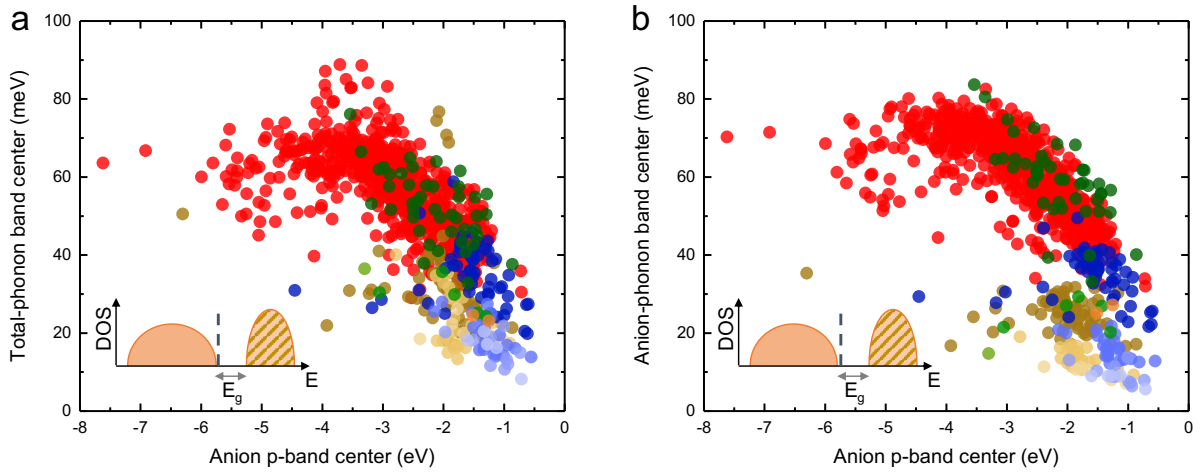

Figure S6. Correlation between a) Total- and b) Anion-phonon band center with the anion p-band centers. Hydrogen-containing compounds (hydrides, hydroxides and amides) were excluded due to the particular low mass of hydrogen and the difference in the nature of bonding which involves the s-orbital instead of p-orbitals. The inset shows the schematic of the anion-projected electronic DOS. The p-band centers were computed by integrating over the occupied states with respect to the top of the valence band indicated by the dashed line. Related to Figure 5.

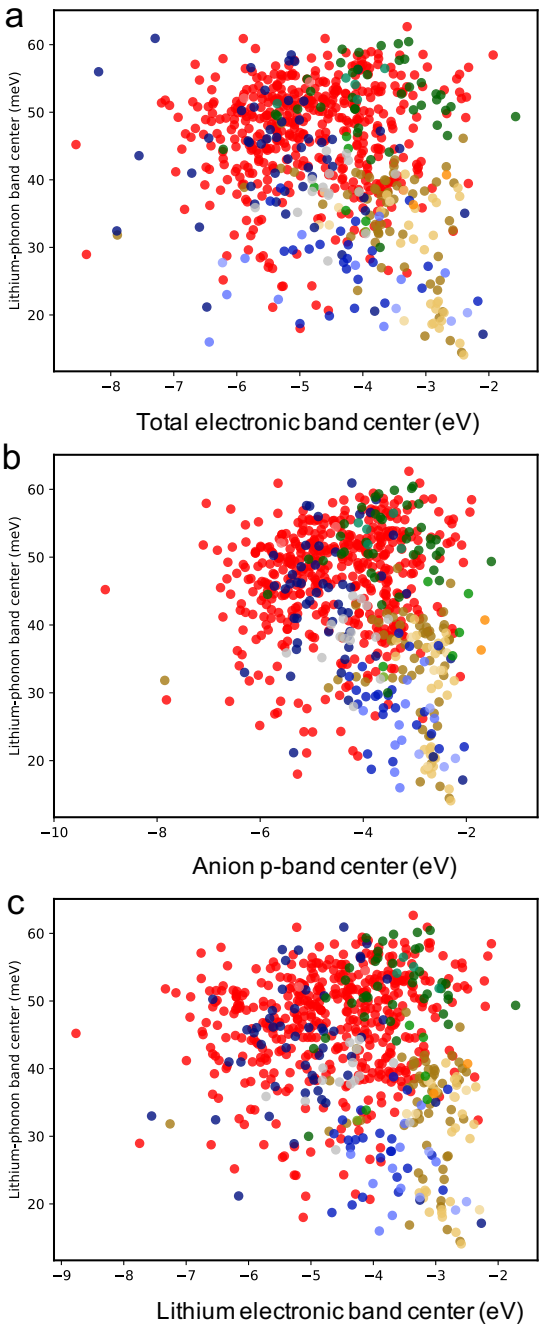

Figure S7. Absence of correlation between Li-phonon band center and a) Total electronic band centers b) anion p-band center and c) Lithium electronic band center. Related to Figure 5 and 6.

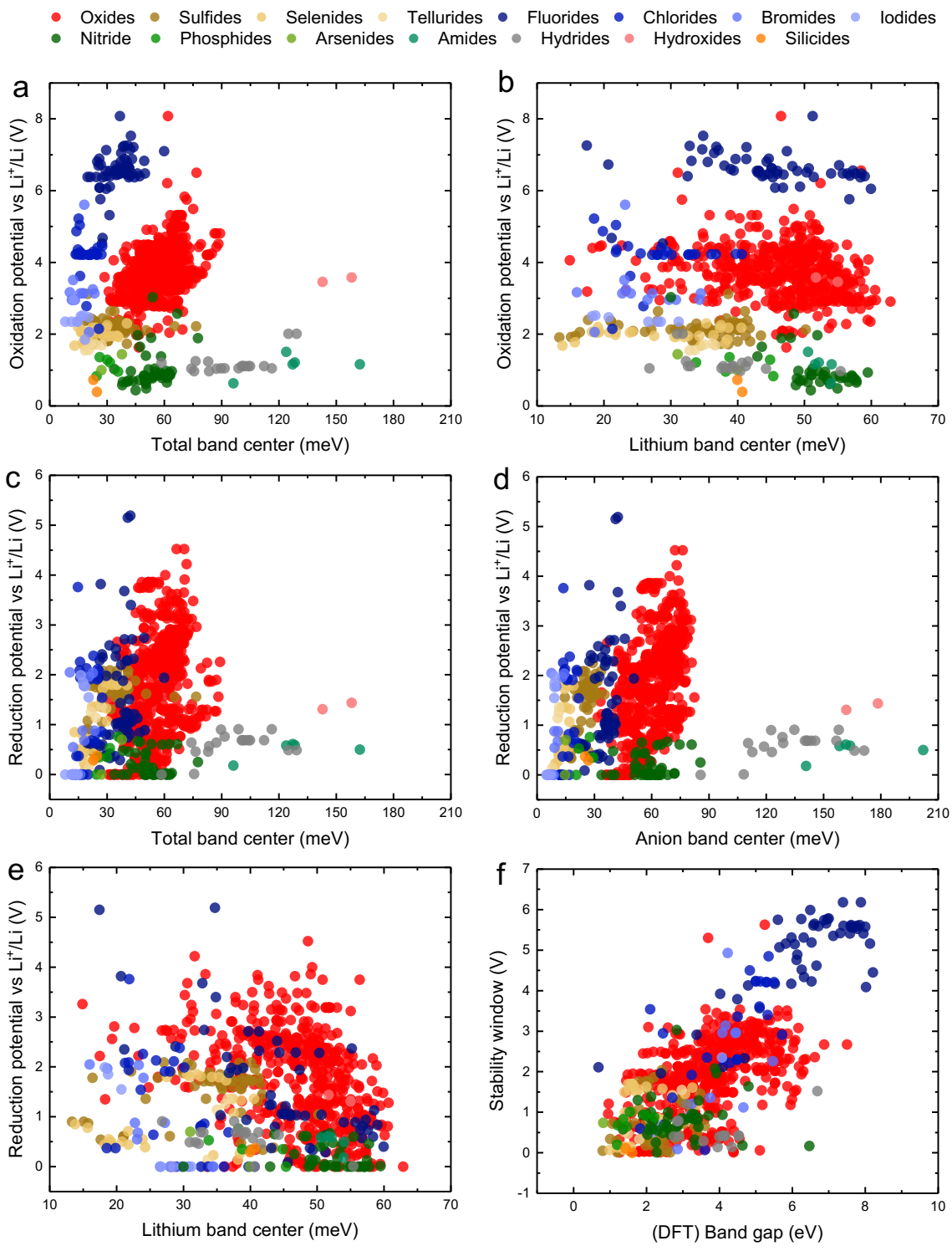

Figure S8. Correlation between oxidation potential and a). Total-phonon band centers b). Lithium-phonon band centers. Correlation between reduction potential and c). Total-phonon band centers d). Anion-phonon band centers e). Lithium-phonon band centers. f). Correlation between stability window and band gaps. Related to Figure 6.

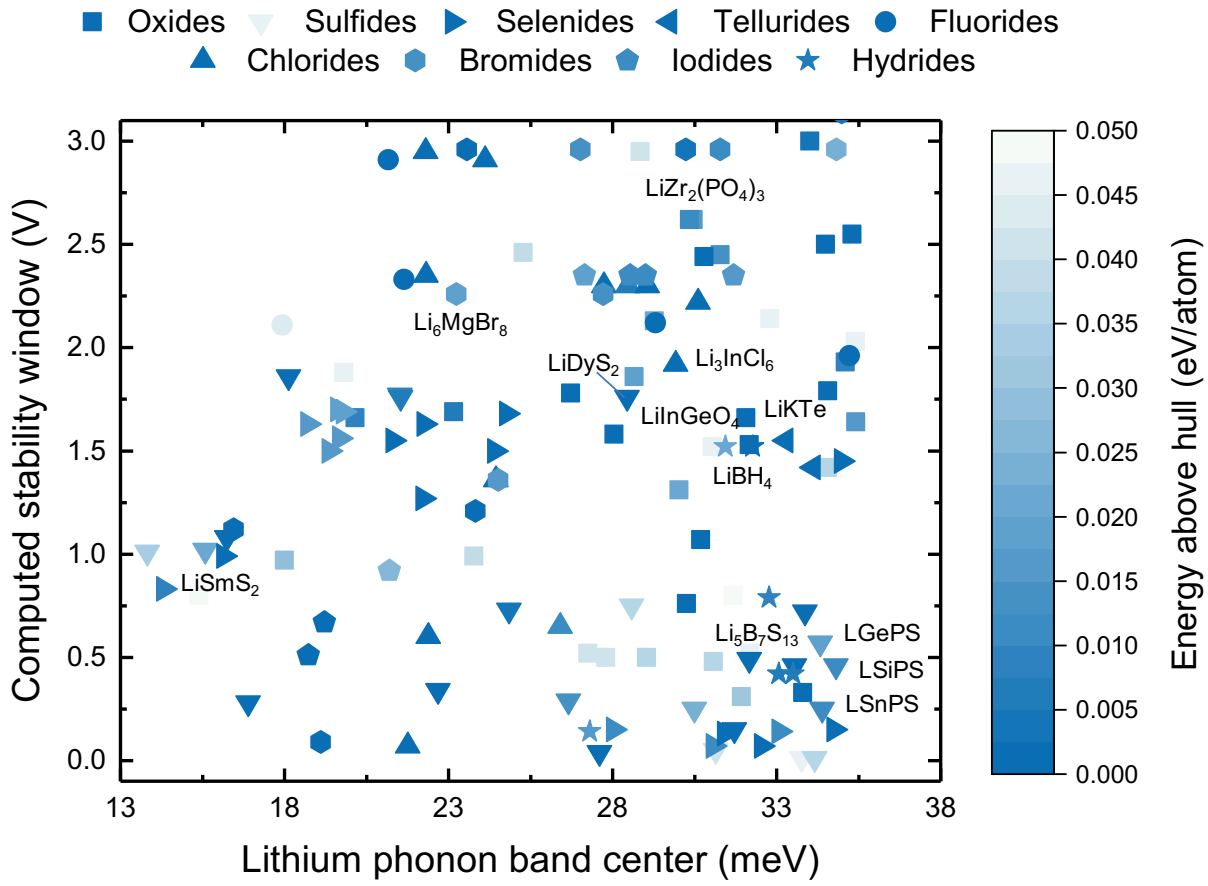

Figure S9. All compounds having stability window smaller than 3V and Li-phonon band center smaller than 35 meV along with their energy above hull. Compounds having non-zero energy above hull are thermodynamically unstable at 0K although they can be stabilized at higher temperature by entropic contributions. LGePS, LSiPS and LSnPS stand respectively for $Li_{10}GeP_2S_{12}$, $Li_{10}SiP_2S_{12}$ and $Li_{10}SnP_2S_{12}$. Related to Figure 7.

Table S1. Compounds with Li-phonon band centers smaller than 35 meV along with their stability window, energy above hull and the material id as appeared in the Materials Project database. Related to Figure 7.

Name	MP id	E_hull (eV/atom)	Li-band centers (meV)	Stability Window (V)
Li2PbO3	mp-22450	0	29.76	0.76
LiNbO3	mp-755559	0.0466	32.297	2.14
LiTa3O8	mp-559908	0.0139	30.778	2.45
LiGdO2	mp-754204	0.0402	28.342	2.95
LiErO2	mp-10971	0.0026	33.518	3
LiTa3O8	mp-7638	0	30.288	2.44
LiNO3	mp-8180	0	34.795	2.55
LiIO3	mp-22955	0.0091	34.595	1.93
LiNb3O8	mp-3368	0	31.571	1.66
LiNbO3	mp-1078377	0.0203	28.772	2.13
LiTa3O8	mp-757158	0.0384	24.783	2.46
LiNb(TeO4)3	mp-758389	0.0015	33.295	0.33
LiGe2(PO4)3	mp-541272	0.0015	27.54	1.58
LiP3W2O13	mp-763452	0.0477	31.178	0.8
Ba4Li(SbO4)3	mp-7971	0	26.219	1.78
LiIn(IO3)4	mp-973966	0	30.187	1.07
LiSn(PO3)3	mp-684503	0.0361	28.535	0.5
LiBiP2O7	mp-684109	0.0451	19.314	1.88
LiSb2P5O16	mp-684104	0.0471	30.541	1.52
LiZr2(PO4)3	mp-681439	0.0159	29.963	2.62
Li2P5WO15	mp-763414	0.0302	31.429	0.31
Li2Sn(PO3)4	mp-26855	0.0416	26.749	0.52
LiSn(PO3)3	mp-26897	0.0406	27.292	0.5
LiInGeO4	mp-17854	0	34.065	1.79
LiP2WO8	mp-763370	0.0488	14.895	0.8
LiSn(PO3)3	mp-758086	0.0464	31.686	0.52
LiZr2(PO4)3	mp-773068	0.0111	29.848	2.62
LiBiP2O7	mp-672979	0.0196	28.165	1.86
LiSn2(PO4)3	mp-562473	0.0053	22.662	1.69
Li2Pr(NO3)5	mp-555979	0	31.056	3.54
LiSbWO6	mp-19694	0.0368	34.053	1.42
LiGa(WO4)2	mp-19695	0.0218	29.531	1.31
LiSi6Bi9O26	mp-757434	0.0381	23.271	0.99
LiB(S2O7)2	mp-1020060	0	31.674	1.53
LiSi6Bi9O26	mp-772721	0.0282	17.502	0.97
Li2TlPCO7	mp-754034	0.0371	30.574	0.48
LiNbSn3(PO4)6	mp-767091	0.0091	19.654	1.66
K2LiTa6(PO8)3	mp-684817	0	33.994	2.5
LiMgAl3(SO4)6	mp-677680	0.017	34.913	1.64
Li3MgPCO7	mp-768190	0.0455	34.902	2.03
LiCa9Mg(PO4)7	mp-686484	0	18.274	3.05
LiCuS	mp-753371	0.0456	33.26	0.01
LiCuS	mp-766467	0.0361	33.657	0.01
LiSmS2	mp-34477	0	15.743	1.08
LiNdS2	mp-36791	0.0204	15.087	1.02

Li2B2S5	mp-29410	0	31.212	0.15
LiPrS2	mp-675419	0.0342	13.322	1.01
Li8Nb2S9	mp-769036	0.0424	30.648	0.05
LiAsS2	mp-555874	0	22.177	0.34
Li5B7S13	mp-532413	0	31.674	0.49
Li3NbS4	mp-769032	0	27.097	0.04
LiHoS2	mp-15790	0	17.622	1.86
LiSbS2	mp-14591	0.0138	26.161	0.29
LiDyS2	mp-15789	0	27.948	1.76
LiYS2	mp-33363	0.0084	21.02	1.77
LiDyS2	mp-33667	0.0069	21.045	1.76
LiSbS2	mp-1079885	0	16.4	0.28
Li7Y7ZrS16	mp-754856	0.0047	24.346	0.73
Li2Ga2GeS6	mp-554782	0.0361	28.086	0.75
Li7Y7Zr9S32	mp-767467	0.0004	33.364	0.72
Li10Sn(PS6)2	mp-721236	0.011	33.891	0.25
Li10Si(PS6)2	mp-720509	0	33.052	0.46
Li10Ge(PS6)2	mp-696138	0.0188	33.833	0.57
Li10Si(PS6)2	mp-696129	0.0112	34.31	0.46
Li10Sn(PS6)2	mp-696123	0.0227	29.995	0.25
RbLiSe	mp-9250	0	34.467	1.45
LiErSe2	mp-35205	0.0176	19.285	1.69
LiSmSe2	mp-35388	0	15.647	0.99
LiDySe2	mp-35717	0.0159	19.175	1.56
LiNdSe2	mp-37605	0.0076	13.81	0.83
LiYSe2	mp-37879	0.0176	19.112	1.7
LiTbSe2	mp-38695	0.0154	18.851	1.5
LiTbSe2	mp-15793	0	23.899	1.5
LiGdSe2	mp-15792	0	21.719	1.27
LiDySe2	mp-15795	0	20.807	1.55
LiHoSe2	mp-15796	0	21.747	1.63
LiErSe2	mp-15797	0	24.262	1.68
LiHoSe2	mp-33322	0.0168	18.208	1.63
Li10Sn(PSe6)2	mp-705516	0.0122	30.561	0.07
Li10Si(PSe6)2	mp-706277	0.0111	27.521	0.15
Li10Si(PSe6)2	mp-721253	0	34.245	0.15
Li10Sn(PSe6)2	mp-721252	0	32.03	0.07
Li10Ge(PSe6)2	mp-721239	0	30.904	0.13
Li10Ge(PSe6)2	mp-696127	0.0114	32.57	0.14
NaLiTe	mp-8754	0	33.621	1.42
KLiTe	mp-4495	0	32.79	1.55
LiAsF6	mp-9144	0	32.837	3.57
LiPF6	mp-9143	0	33.088	4.09
LiCuF4	mp-753541	0.0441	17.426	2.11
LiBiF6	mp-27419	0	34.716	1.96
LiSbF6	mp-3980	0	34.861	4.13
Cs2LiTlF6	mp-989562	0	20.661	2.91
LiTl2InF6	mp-989551	0	28.812	2.12
LiTl2GaF6	mp-989577	0	21.141	2.33
K2LiAlF6	mp-9839	0.0015	32.535	5.6

LiSnCl3	mp-998230	0.0109	25.901	0.65
Li3ErCl6	mp-676361	0	25.508	3.61
CsLiCl2	mp-23364	0	33.689	4.23
Li2ZnCl4	mp-23416	0.001	27.234	2.3
LiYb2Cl5	mp-23421	0.0189	28.914	4.21
Li2CdCl4	mp-38008	0	30.108	2.22
Li2MgCl4	mp-38684	0	32.655	3.4
LiGaCl3	mp-29344	0	21.256	0.07
CsLi3Cl4	mp-571666	0.0124	28.001	4.21
Li3InCl6	mp-676109	0	29.424	1.92
CsLi2Cl3	mp-569117	0.0042	32.635	4.21
Li10Mg7Cl24	mp-530738	0.0027	33.118	3.36
Li2ZnCl4	mp-22961	0.0053	27.967	2.3
LiGaCl4	mp-28341	0	28.563	2.3
LiAlCl4	mp-22983	0	23.62	2.91
Rb2LiInCl6	mp-989583	0	21.803	2.95
Rb2LiTlCl6	mp-989579	0	21.888	0.6
LiTl2InCl6	mp-989512	0	23.941	1.36
Cs2LiInCl6	mp-571527	0	21.815	2.35
Cs2LiYCl6	mp-567652	0	19.831	4.5
Cs2LiLuCl6	mp-570379	0	18.524	4.85
CsLi2Br3	mp-606680	0.0137	26.519	2.96
Li2ZnBr4	mp-28829	0.0172	24.016	1.36
Li6MgBr8	mp-29008	0.0199	22.737	2.26
Li3ErBr6	mp-37873	0	23.178	4.93
Cs2Li3Br5	mp-571409	0.0108	30.78	2.96
RbLiBr2	mp-28237	0.0048	34.486	3.14
LiGaBr4	mp-28326	0	23.315	1.21
LiGaBr3	mp-28327	0	18.607	0.09
CsLiBr2	mp-23057	0.0046	29.73	2.96
Cs2LiBr3	mp-1095674	0.0231	34.317	2.96
Li2MgBr4	mp-29009	0.0145	27.22	2.26
Cs2LiInBr6	mp-989405	0	15.956	1.12
Rb2LiDyBr6	mp-567628	0	23.059	2.96
Cs2Li3I5	mp-608311	0.0113	28.504	2.35
Li2ZnI4	mp-23497	0.0263	20.704	0.92
LiGaI4	mp-567967	0	18.723	0.67
LiInI4	mp-541001	0	18.231	0.51
Cs2Li3I5	mp-1080534	0.0115	28.035	2.35
Cs3LiI4	mp-569238	0.0183	26.648	2.35
CsLi2I3	mp-569055	0.0174	31.189	2.35
Sr4Li(BN2)3	mp-9723	0	29.999	3.03
LiBeP	mp-9915	0	33.782	0.68
LiBeAs	mp-9562	0	31.011	0.74
LiBeH3	mp-977148	0.0051	32.572	0.42
LiAlH4	mp-976291	0.0167	26.807	0.14
LiBH4	mp-30209	0	31.774	1.52
LiBeH3	mp-1079676	0.006	32.998	0.42
LiBH4	mp-1095543	0.0206	30.941	1.52
K2LiAlH6	mp-24411	0.0091	32.272	0.79

Transparent methods

Database and screening criteria

The structure of all compounds in our study were sourced from the Materials Project database(Jain et al., 2013) containing ~ 14,000 Li-containing compounds using the API functionality(Ong et al., 2015) implemented in the *Pymatgen* software package.(Ong et al., 2013) Four criteria were used to pre-screen all these compounds before proceeding to the computation of phonon band centers: (1) The stability of each compound was assessed based on their energy above hull, E_{hull} which is the distance between the point representing the compound in the phase diagram and the convex hull.(Ong et al., 2010; Ping Ong et al., 2008) Materials having $E_{hull} > 0$ are thermodynamically unstable at 0 K. However, if E_{hull} is not too large, the material can still be stable at finite temperatures due to the entropic contribution to the free energy. We set the threshold of E_{hull} to 50 meV/atom based on the observation that e.g. LGPS (space group $P4_2mc$) has $E_{hull} = 30$ meV/atom but can still be synthesized and is stable RT.(Kamaya et al., 2011) (2) The next criterion was to have a computed band gap of at least 1 eV in order to filter out compounds with too high electronic conductivity to be used as electrolytes. (3) We included only ternary, quaternary and quintenary compounds and excluded the binary compounds due to their rather restricted chemical space. (4) Finally, we excluded all compounds containing 3d transition elements, platinum-group elements and elements in the actinide series, due to concerns about cost, toxicity and internal redox-activity. After this pre-screening, ~ 1200 compounds were retained, and their phonon band center computed.

Detailed methodology of *Quickhess* method

The main idea of this method is that the eigenvalues of the Hessian matrix can be estimated with a single DFT force projection if reasonably good approximations to the eigenvectors are available. In the original implementation (Voss and Vegge, 2008) approximate eigenvectors were constructed from a point charge force field evaluated with Ewald summation and thus with negligible effort compared to a DFT calculation, and point charges were optimized to reproduce the DFT ground-state ionic positions. Here, instead of using Ewald summation, we screen the Coulomb interaction: $V_{screen} \sim exp(-Kr)/r$ with K=1/2Å^{-1} and sum in real space only. Charges are

not fitted but we simply use Bader charges. Neither of the two simplifications changes the trends in approximated phonon band centers. Following Voss *et al.* (Voss and Vegge, 2008), the Hessian matrix of this purely electrostatic force field is diagonalized to obtain the eigenvalues and eigenvectors (displacements) $\underline{u_i}$. From these eigenvectors, a special displacement $\underline{w}$ is constructed simply as a sum of all $\underline{u_i}$. The more accurate Hessian $\boldsymbol{H}$ eigenvalues h_i can be obtained by projecting the Hessian of a more accurate DFT Hamiltonian onto this displacement:

$$h_i \approx \underline{u_i}^{\mathrm{T}} \boldsymbol{H} \underline{w} \tag{S1}$$

The projection of the Hessian $\boldsymbol{H}$ onto $\underline{w}$ is approximated as the difference between the force on a new displaced configuration of the initial structure which is generated by applying the displacement $\underline{w}$ to the structure and the force on the initial structure:

$$\boldsymbol{H}\underline{w} \approx \frac{1}{\varepsilon}\left[\underline{\nabla}E\left(\underline{r_o} + \varepsilon\underline{w}\right) - \underline{\nabla}E\left(\underline{r_o}\right)\right] \tag{S2}$$

Where E is the (DFT) energy and $\underline{r_o}$ are the ground state coordinates and ε is a parameter to scale the displacement for the finite difference as defined in equation (2). If the initial configuration is a well relaxed structure, then the term $\underline{\nabla}E\left(\underline{r_o}\right)$ can be neglected. The parameter ε must be chosen carefully such that the induced force is well above numerical noise in the DFT calculations but also not too large potentially invalidating the harmonic approximation.

Synthesis and characterization of Li_3ErCl_6

The preparations and sample treatment for all compounds were carried out under argon atmosphere. Erbium chloride ($ErCl_3$, anhydrous, 99.9 %, Alfa Aesar) and lithium chloride (LiCl, ultra-dry, 99.9 %, Alfa Aesar) were mixed in the appropriate stoichiometric molar ratios, while adding approximately 2 wt% excess $ErCl_3$ relative to the total weighted mass to counter the loss of $ErCl_3$ during the hand grinding procedure. The mixture was then hand ground in an agate mortar to homogenize the powders and afterwards loaded into ball mill vials with a 30:1 mass ratio of the ZrO_2 milling media (3 mm in diameter) to the starting powder. The precursors were milled for 297 total cycles, while one cycle consists of 5 minutes of milling, followed by 15 minutes of rest time. Additionally, after every 99th cycle, the cups were opened and the powder homogenized manually

again to reduce the loss of sample on the inner walls of the vials. Crystallization of the as-prepared amorphous compounds were achieved by subsequent annealing for 1 h at 550 °C.

X-ray powder diffraction was carried out using an Empyrean powder diffractometer (PANalytical, Netherlands) with CuKa radiation (λ_1 = 1.54051 Å, λ_2 = 1.54051 Å) in Bragg–Brentano θ–θ geometry, and a PIXcel3D area detector with 255 measuring channels. Powder samples were placed on (911)-oriented silicon zero background holders that were sealed with Kapton foil under an argon atmosphere. Patterns were collected in the range of 10–90° 2θ with a step size of 0.026 and an exposure time of 150 s per step for the ball milled sample and 425 s for the subsequently annealed sample, to achieve a sufficiently high intensity and therefore acquire reliable lattice parameter values. Pawley fits(Pawley, 1981) were performed using the TOPAS-Academic V6 software package (Coelho, 2018). A manual background using 62 points was used, whereas the peak profiles were described by a Thompson–Cox–Hastings pseudo-Voigt function.

The ionic conductivities were measured by AC impedance spectroscopy, using pellets (1.4 mm average thickness, >80 % density for the amorphous compound (>75 % for the crystalline compound)) with vapor deposited gold layers (200 nm on each side; surface area of 0.53 cm^2). Electrochemical impedance analysis (EIS) was conducted in the temperature range of -40 °C to 60 °C using a VMP300 impedance analyzer (Biologic) at frequencies from 7 MHz to 100 mHz with an amplitude of 10 mV. All measurements were performed in pouch cells under an argon atmosphere.

Supplemental references

Coelho, A.A., 2018. *TOPAS* and *TOPAS-Academic* : an optimization program integrating computer algebra and crystallographic objects written in C++. Journal of Applied Crystallography 51, 210–218. https://doi.org/10.1107/S1600576718000183

Jain, A., Ong, S.P., Hautier, G., Chen, W., Richards, W.D., Dacek, S., Cholia, S., Gunter, D., Skinner, D., Ceder, G., Persson, K.A., 2013. Commentary: The Materials Project: A materials genome approach to accelerating materials innovation. APL Materials 1, 011002. https://doi.org/10.1063/1.4812323

Kamaya, N., Homma, K., Yamakawa, Y., Hirayama, M., Kanno, R., Yonemura, M., Kamiyama, T., Kato, Y., Hama, S., Kawamoto, K., Mitsui, A., 2011. A lithium superionic conductor. Nat Mater 10, 682–686. https://doi.org/10.1038/nmat3066

Ong, S.P., Cholia, S., Jain, A., Brafman, M., Gunter, D., Ceder, G., Persson, K.A., 2015. The Materials Application Programming Interface (API): A simple, flexible and efficient API for materials data based on REpresentational State Transfer (REST) principles. Computational Materials Science 97, 209–215. https://doi.org/10.1016/j.commatsci.2014.10.037

Ong, S.P., Jain, A., Hautier, G., Kang, B., Ceder, G., 2010. Thermal stabilities of delithiated olivine MPO4 (M=Fe, Mn) cathodes investigated using first principles calculations. Electrochemistry Communications 12, 427–430. https://doi.org/10.1016/j.elecom.2010.01.010

Ong, S.P., Richards, W.D., Jain, A., Hautier, G., Kocher, M., Cholia, S., Gunter, D., Chevrier, V.L., Persson, K.A., Ceder, G., 2013. Python Materials Genomics (pymatgen): A robust, open-source python library for materials analysis. Computational Materials Science 68, 314–319. https://doi.org/10.1016/j.commatsci.2012.10.028

Pawley, G.S., 1981. Unit-cell refinement from powder diffraction scans. Journal of Applied Crystallography 14, 357–361. https://doi.org/10.1107/S0021889881009618

Ping Ong, S., Wang, L., Kang, B., Ceder, G., 2008. Li−Fe−P−O2 Phase Diagram from First Principles Calculations. Chem. Mater. 20, 1798–1807. https://doi.org/10.1021/cm702327g

Voss, J., Vegge, T., 2008. Γ-point lattice free energy estimates from O(1) force calculations. The Journal of Chemical Physics 128, 184708. https://doi.org/10.1063/1.2919122